

Frames and vertex-frequency representations in graph fractional Fourier domain

Linbo Shang and Zhichao Zhang, *Member, IEEE*

Abstract—Vertex-frequency analysis, particularly the windowed graph Fourier transform (WGFT), is a significant challenge in graph signal processing. Tight frame theories is known for its low computational complexity in signal reconstruction, while fractional order methods shine at unveil more detailed structural characteristics of graph signals. In the graph fractional Fourier domain, we introduce multi-windowed graph fractional Fourier frames (MWGFRFF) to facilitate the construction of tight frames. This leads to developing the multi-windowed graph fractional Fourier transform (MWGFRFT), enabling novel vertex-frequency analysis methods. A reconstruction formula is derived, along with results concerning dual and tight frames. To enhance computational efficiency, a fast MWGFRFT (FMWGFRFT) algorithm is proposed. Furthermore, we define shift multi-windowed graph fractional Fourier frames (SMWGFRFF) and their associated transform (SMWGFRFT), exploring their dual and tight frames. Experimental results indicate that FMWGFRFT and SMWGFRFT excel in extracting vertex-frequency features in the graph fractional Fourier domain, with their combined use optimizing analytical performance. Applications in signal anomaly detection demonstrate the advantages of FMWGFRFT.

Index Terms—Frames, multi-windowed, tight frames, vertex-frequency representation, graph fractional Fourier domain.

I. INTRODUCTION

SIGNAL processing (SP) focuses on analyzing and processing information defined in Euclidean domains. However, with the rapid advancement of communication technologies and data proliferation [1], modern applications often encounter information residing in non-Euclidean domains. SP techniques struggle to address the irregular nature of these domains. Graph signal processing (GSP) [2], [3], [4], [5], [6], [7] generalizes SP to signals defined on non-Euclidean domains, effectively capturing topological structures through weighted graphs. A central challenge in GSP lies in designing dictionaries of atoms and transform methods for accurately identifying

and utilizing graph topology. Existing approaches primarily rely on graph adjacency matrices rooted in algebraic signal processing and Laplacian matrices derived from spectral graph theory [8]. Currently, the GSP theory mainly includes the following: graph Fourier transform (GFT) [1], [9], graph filters [10], [11], graph sampling and recovery [12], [13], frequency analysis [4], and fast algorithms [14], [15], [16]. These results have been applied to social networks and sensor networks and extended to machine learning.

Vertex-frequency analysis is a significant challenge in GSP. Due to the classical Fourier transform's limitation in capturing time-varying properties, the windowed Fourier transform, also known as short-time Fourier transform, has become a crucial time-frequency analysis tool in SP. Similarly, because GFT is ineffective for vertex-frequency representation, the windowed graph Fourier transform (WGFT) [17], [18], [19], [20], [21], [22], [23] is proposed. Various operators related to WGFT are discussed [17], [19], including the convolution operator, modulation operator and translation operator. [17] also construct windowed graph Fourier frames (WGFF), i.e., dictionaries of atoms adapted to the underlying graph structure, facilitating effective vertex-frequency analysis. If WGFF is tight, the spectrogram can be interpreted as an energy density function of the signal over the vertex-frequency plane [17].

Leveraging the knowledge of frames [24], we understand that signal reconstruction requires an additional dual frame calculation. By applying tight frames, the need for dual frame calculations can be eliminated, thereby saving the extra computational cost associated with dual frames. To facilitate the construction of tight frames, multi-windowed graph Fourier frames (MWGFF) [25] are introduced to develop novel vertex-frequency analysis methods. The MWGFF and shift multi-windowed graph Fourier frames are utilized to extract vertex-frequency features of signals in the graph Fourier domain. However, MWGFF is typically ineffective in processing signals in the graph fractional Fourier domain.

To obtain more detailed structural properties of graph signals, a fractional order [26], [27], [28], [29], [30], [31], [32] is adopted. Fractional graph signal processing is a nascent field that extends GSP techniques by incorporating fractional orders. The graph fractional Fourier domain—a combination of the fractional transform domain and graph spectral domain—has typically been explored as a potentially enriching research topic. GFRFT [33] and SGFRFT [32] are advantageous for revealing local features of graph signals. The windowed graph fractional Fourier transform (WGFRFT) [34] is introduced to extract vertex-frequency information from signals on weighted graphs. However, WGFRFT cannot effectively extract vertex-frequency information for a fixed window function.

This work was supported in part by the Foundation of Key Laboratory of System Control and Information Processing, Ministry of Education under Grant Scip20240121; in part by the Foundation of Key Laboratory of Computational Science and Application of Hainan Province under Grant JSKX202401; and in part by the Foundation of Key Laboratory of Numerical Simulation of Sichuan Provincial Universities under Grant KLNS-2024SZFZ005. (*Corresponding author: Zhichao Zhang.*)

Linbo Shang is with the School of Mathematics and Statistics, Nanjing University of Information Science and Technology, Nanjing 210044, China (e-mail: ahanglinbo@163.com).

Zhichao Zhang is with the School of Mathematics and Statistics, Nanjing University of Information Science and Technology, Nanjing 210044, China, with the Key Laboratory of System Control and Information Processing, Ministry of Education, Shanghai Jiao Tong University, Shanghai 200240, China, with the Key Laboratory of Computational Science and Application of Hainan Province, Hainan Normal University, Haikou 571158, China, and also with the Key Laboratory of Numerical Simulation of Sichuan Provincial Universities, School of Mathematics and Information Sciences, Neijiang Normal University, Neijiang 641000, China (e-mail: zzc910731@163.com).

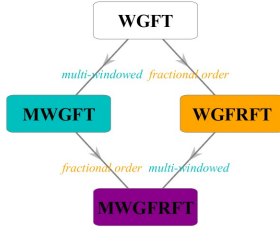


Fig. 1. Relationships among WGFT [17], MWGFT [25], WGRFT [34], and MWGRFT.

In summary, traditional vertex-frequency analysis methods fail to extract vertex-frequency features in the graph fractional Fourier domain for given window functions. To overcome these limitations, we propose the multi-windowed graph fractional Fourier transform (MWGRFT), which combines the advantages of multi-window and fractional orders. MWGRFT is a generalized transform that includes WGFT [17], MWGFT [25], and WGRFT [34], as illustrated in Fig. 1. With its additional parameters l and α , MWGRFT provides enhanced flexibility and adaptability. The main contributions of our work can be summarized as follows:

- Based on the graph fractional translation operator and the graph fractional modulation operator, we obtain a multi-windowed graph fractional Fourier frame (MWGRFF). Similarly, by applying the graph fractional shift operator and the graph fractional modulation operator, we present a shift multi-windowed graph fractional Fourier frame (SMWGRFF).
- The MWGRFT and the shift multi-windowed graph fractional Fourier transform (SMWGRFT) are defined to obtain a vertex-frequency representation in the graph fractional Fourier domain for given window functions.
- We propose a fast MWGRFT (FMWGRFT) algorithm designed to significantly enhance computational efficiency.
- We derive dual frames and tight frames corresponding to MWGRFF and SMWGRFF, and also provide a reconstruction formula.
- In the graph fractional Fourier domain, we demonstrate an application of signal anomaly detection by applying WGFT [17], MWGFT [25], WGRFT [34], SMWGRFT, SMWGRFT, and FMWGRFT. The results highlight the effectiveness of FMWGRFT in accurately identifying anomalous vertices.

The main connections and differences between the current study and previous ones are concluded as follows:

- These studies focus on vertex-frequency representations, aiming to extract detailed vertex and frequency features.
- WGFT [17], MWGFT [25], and WGRFT [34] are special cases of the current study. The current study addresses the limitation of WGFT, i.e., its inability to extract detailed vertex or frequency features; The current study overcomes the limitation of MWGFT, which cannot effectively perform frequency feature extraction; The

current study resolves the limitation of WGRFT, i.e., its inability to effectively extract vertex features.

The remaining sections are organized as follows. Section II provides a brief review of the background relevant to this study. In Section III, we define MWGRFF and present several results related to tight frames and introduce the concept of MWGRFT. In Section IV, we propose a fast MWGRFT (FMWGRFT) algorithm. Section V presents results concerning the dual of MWGRFF and a reconstruction formula. In Section VI, we define SMWGRFF and discuss related dual and tight frames. In addition, we introduce the SMWGRFT concept. In Section VII, the construction of tight MWGRFF and SMWGRFF is exemplified. In Section VIII, the experimental results are presented. Section IX presents the applications related to anomaly detection. Finally, Section X concludes this study.

II. PRELIMINARIES

A. Spectral graph theory

An undirected weighted graph $\mathcal{G} = \{\mathcal{V}, \mathcal{E}, W\}$ consists of a finite set of vertices \mathcal{V} , where N is the number of vertices, \mathcal{E} is a set of edges and W is a weighted adjacency matrix. The non-normalized graph Laplacian is a symmetric difference operator $\mathcal{L} = D - W$ [35], where D is a diagonal degree matrix. Suppose that the corresponding Laplacian eigenvalues are arranged in ascending order as: $0 = \lambda_0 < \lambda_1 \leq \lambda_2 \leq \dots \leq \lambda_{N-1} := \lambda_{max}$. Therefore, $\mathcal{L} = \chi \Lambda \chi^H$, where the superscript H denotes the Hermitian transpose operation, $\chi = [\chi_0, \chi_1, \dots, \chi_{N-1}]$ is a unitary column matrix and $\Lambda = \text{diag}([\lambda_0, \lambda_1, \dots, \lambda_{N-1}])$ is a diagonal matrix.

For a signal $\mathbf{f} = [f(1), f(2), \dots, f(N)]^T$ defined on the graph \mathcal{G} , the GFT of \mathbf{f} is

$$\hat{\mathbf{f}}(\lambda_k) = \langle \mathbf{f}, \chi_k \rangle = \sum_{n=1}^N f(n) \chi_k^*(n), k = 0, 1, \dots, N-1.$$

The inverse GFT is given by

$$f(n) = \sum_{k=0}^{N-1} \hat{\mathbf{f}}(\lambda_k) \chi_k(n), n = 1, 2, \dots, N.$$

We observe that GFT is represented by the matrix χ ; as an extension, the spectral graph fractional Fourier transform (SGFRFT) is represented as χ^α . The graph fractional Laplacian operator $\mathcal{L}_\alpha = \gamma R \gamma^H$, where $0 < \alpha \leq 1$ [32]. Note that χ is unitary then $\gamma = [\gamma_0, \gamma_1, \dots, \gamma_{N-1}] = \chi^\alpha$ is also unitary. And $R = \text{diag}([r_0, r_1, \dots, r_{N-1}]) = \Lambda^\alpha$, so that $r_k = \lambda_k^\alpha$ for $k = 0, 1, \dots, N-1$. The SGFRFT of a signal \mathbf{f} defined on the graph \mathcal{G} is expressed as [32]:

$$\hat{\mathbf{f}}_\alpha(r_k) = \sum_{n=1}^N f(n) \gamma_k^*(n), k = 0, 1, \dots, N-1,$$

when $\alpha = 1$, the SGFRFT degenerates into GFT. The inverse SGFRFT is given by

$$f(n) = \sum_{k=0}^{N-1} \hat{\mathbf{f}}_\alpha(r_k) \gamma_k(n), n = 1, 2, \dots, N.$$

The Parseval relation for the SGFRFT holds. For any signals \mathbf{f} and \mathbf{g} defined on the graph \mathcal{G} , we have $\langle \mathbf{f}, \mathbf{g} \rangle = \langle \hat{\mathbf{f}}_\alpha, \hat{\mathbf{g}}_\alpha \rangle$.

B. Windowed graph fractional Fourier transform[34]

Definition 1. (Graph fractional translation operator) For any signal \mathbf{g} defined on the graph \mathcal{G} and $i \in \{1, 2, \dots, N\}$, the graph fractional translation operator T_i^α is defined as

$$(T_i^\alpha \mathbf{g})(n) = (\sqrt{N})^\alpha \sum_{p=0}^{N-1} \hat{\mathbf{g}}_\alpha(r_p) \gamma_p^*(i) \gamma_p(n). \quad (1)$$

Definition 2. (Graph fractional modulation operator) For any signal \mathbf{g} defined on the graph \mathcal{G} and $k \in \{0, 1, \dots, N-1\}$, define the graph fractional modulation operator by

$$(M_k^\alpha \mathbf{g})(n) = (\sqrt{N})^\alpha \mathbf{g}(n) \gamma_k(n).$$

The windowed graph fractional Fourier atoms generated by a window function \mathbf{g} on \mathcal{G} are defined by

$$\mathbf{g}_{i,k}^{(\alpha)}(n) = (M_k^\alpha T_i^\alpha \mathbf{g})(n) = N^\alpha \gamma_k(n) \sum_{p=0}^{N-1} \hat{\mathbf{g}}_\alpha(r_p) \gamma_p^*(i) \gamma_p(n),$$

where $i = 1, 2, \dots, N$ and $k = 0, 1, \dots, N-1$. We denote the set of windowed graph fractional Fourier atoms by

$$\mathcal{G}_\alpha^w = \{\mathbf{g}_{i,k}^{(\alpha)}\}_{i=1,2,\dots,N; k=0,1,\dots,N-1; 0 < \alpha \leq 1}. \quad (2)$$

Definition 3. (Windowed graph fractional Fourier transform) Given a window function $\mathbf{g} \in \mathbb{C}^N$, the SGFRFT of \mathbf{g} is $\hat{\mathbf{g}}_\alpha$. For a signal \mathbf{f} , the WGRFT of \mathbf{f} is denoted by

$$Wf(\mathbf{g}_{i,k}^{(\alpha)}) = N^\alpha \sum_{n=1}^N f(n) \left(\sum_{p=0}^{N-1} \hat{\mathbf{g}}_\alpha^*(r_p) \gamma_p(i) \gamma_p^*(n) \right) \gamma_k^*(n).$$

C. Frames and operators[24]

A frame is a collection of vectors that span the signal space, providing a redundant representation of signals. This redundancy can be utilized to facilitate signal reconstruction.

Definition 4. A family of vectors $\{\mathbf{f}_k\}_{k=1}^M \subseteq \mathbb{C}^N$ ($M \geq N$) is a finite frame for \mathbb{C}^N if there exist constants $A, B > 0$ such that

$$A \|\mathbf{f}\|^2 \leq \sum_{k=1}^M |\langle \mathbf{f}, \mathbf{f}_k \rangle|^2 \leq B \|\mathbf{f}\|^2$$

holds for every $\mathbf{f} \in \mathbb{C}^N$.

The constants A and B are called frame bounds, and if $A = B$, $\{\mathbf{f}_k\}_{k=1}^M$ is called a tight frame. For a tight frame $\{\mathbf{f}_k\}_{k=1}^M$ with frame bound C_0 , the following reconstruction formula holds:

$$\mathbf{f} = \frac{1}{C_0} \sum_{k=1}^M \langle \mathbf{f}, \mathbf{f}_k \rangle \mathbf{f}_k, \quad \mathbf{f} \in \mathbb{C}^N.$$

For a frame $\{\mathbf{f}_k\}_{k=1}^M$, define its synthesis operator by $T(\{c_k\}) = \sum_{k=1}^M c_k \mathbf{f}_k$ and the analysis operator by $T^* \mathbf{f} = \{\langle \mathbf{f}, \mathbf{f}_k \rangle\}$. Integrating T and T^* together, which forms a pair of dual operators, define the frame operator of $\{\mathbf{f}_k\}$ by $S = TT^*$, i.e.

$$S\mathbf{f} = \sum_{k=1}^M \langle \mathbf{f}, \mathbf{f}_k \rangle \mathbf{f}_k, \quad \mathbf{f} \in \mathbb{C}^N,$$

which is a positive, bounded, invertible and self-adjoint operator.

If there exists another sequence of vectors $\{\mathbf{g}_k\}_{k=1}^M$ such that

$$\mathbf{f} = \sum_{k=1}^M \langle \mathbf{f}, \mathbf{g}_k \rangle \mathbf{f}_k, \quad \mathbf{f} \in \mathbb{C}^N,$$

then $\{\mathbf{g}_k\}_{k=1}^M$ is called a dual frame of $\{\mathbf{f}_k\}_{k=1}^M$.

III. MULTI-WINDOWED GRAPH FRACTIONAL FOURIER FRAMES

In this section, we introduce multi-windowed graph fractional Fourier frames (MWGFRFF) and discuss related tight frames. Furthermore, we define multi-windowed graph fractional Fourier transforms (MWGFRFT).

Analogue to (2), for a finite sequence of window functions $\mathbf{g}_1, \mathbf{g}_2, \dots, \mathbf{g}_L \in \mathbb{C}^N$, the SGFRFT of \mathbf{g}_l is $\hat{\mathbf{g}}_{l\alpha}$, we define the set of multi-windowed graph fractional Fourier atoms by

$$\mathcal{G}_{l\alpha}^w = \{\mathbf{g}_{i,k}^{(l\alpha)}\}_{i=1,2,\dots,N; k=0,1,\dots,N-1; l=1,2,\dots,L; 0 < \alpha \leq 1}, \quad (3)$$

where

$$\mathbf{g}_{i,k}^{(l\alpha)}(n) = (M_k^\alpha T_i^\alpha \mathbf{g}_l)(n) = N^\alpha \gamma_k(n) \sum_{p=0}^{N-1} \hat{\mathbf{g}}_{l\alpha}(r_p) \gamma_p^*(i) \gamma_p(n).$$

Theorem 1. Let $\mathcal{G}_{l\alpha}^w$ be the set of multi-windowed graph fractional Fourier atoms defined in (3). If $\sum_{l=1}^L |\hat{\mathbf{g}}_{l\alpha}(0)|^2 \neq 0$, then $\mathcal{G}_{l\alpha}^w$ is a frame (i.e., MWGFRFF), thus for any signal $\mathbf{f} \in \mathbb{C}^N$,

$$0 < A \|\mathbf{f}\|_2^2 \leq \sum_{l=1}^L \sum_{i=1}^N \sum_{k=0}^{N-1} |\langle \mathbf{f}, \mathbf{g}_{i,k}^{(l\alpha)} \rangle|^2 \leq B \|\mathbf{f}\|_2^2 < \infty,$$

where lower frame bound

$$0 < A = \min_{n \in \{1, 2, \dots, N\}} \left\{ N^\alpha \sum_{l=1}^L \|T_n^\alpha \mathbf{g}_l\|_2^2 \right\}, \quad (4)$$

and upper frame bound

$$B = \max_{n \in \{1, 2, \dots, N\}} \left\{ N^\alpha \sum_{l=1}^L \|T_n^\alpha \mathbf{g}_l\|_2^2 \right\} < \infty. \quad (5)$$

Proof. See Appendix A. \square

Let $\mathbf{c} = (c_1, \dots, c_N)^T$, where $c_n = N^\alpha \sum_{l=1}^L \|T_n^\alpha \mathbf{g}_l\|_2^2$. By Appendix A, Eq. (15) shows that $\langle S\mathbf{f}, \mathbf{f} \rangle = \langle \mathbf{c} \circ \mathbf{f}, \mathbf{f} \rangle$, $\mathbf{f} \in \mathbb{C}^N$, where \circ denotes the entrywise product. Equivalently, we have

$$S\mathbf{f} = \mathbf{c} \circ \mathbf{f} = \mathbf{D}_c \mathbf{f}, \quad \mathbf{f} \in \mathbb{C}^N, \quad (6)$$

where $\mathbf{D}_c = \text{diag}(\mathbf{c})$ is a diagonal matrix, with its n th diagonal entry $D_{nn} = c_n$.

Corollary 1. $\mathcal{G}_{l\alpha}^w$ is a tight frame if and only if there exists a constant C such that $N^\alpha \sum_{l=1}^L \|T_n^\alpha \mathbf{g}_l\|_2^2 = C$ for $n = 1, 2, \dots, N$.

Proof. See Appendix B. \square

Corollary 2. Let $\mathcal{G}_{l\alpha}^w$ be the set of multi-windowed graph fractional Fourier atoms defined in (3). If there exists a constant

C such that $\sum_{l=1}^L |\hat{\mathbf{g}}_{l\alpha}(r_p)|^2 = C$ for $p = 0, 1, \dots, N-1$, then $\mathcal{G}_{l\alpha}^w$ is a tight frame with frame bounds $A = B = N^{2\alpha}C$.

Proof. See Appendix C. \square

Definition 5. (Multi-windowed graph fractional Fourier transform) Given window functions $\mathbf{g}_1, \dots, \mathbf{g}_L \in \mathbb{R}^N$, the SGFRFT of \mathbf{g}_l is $\hat{\mathbf{g}}_{l\alpha}$. Let $\mathcal{G}_{l\alpha}^w$ is a multi-windowed graph fractional Fourier frame defined in Theorem 1. For a signal $\mathbf{f} \in \mathbb{C}^N$, the MWGFRFT $Wf(\mathbf{g}_{i,k}^{(l\alpha)}) := \langle \mathbf{f}, \mathbf{g}_{i,k}^{(l\alpha)}(n) \rangle$ of \mathbf{f} is

$$Wf(\mathbf{g}_{i,k}^{(l\alpha)}) = N^\alpha \sum_{l=1}^L \sum_{n=1}^N f(n) \left(\sum_{p=0}^{N-1} \hat{\mathbf{g}}_{l\alpha}^*(r_p) \gamma_p(i) \gamma_p^*(n) \right) \gamma_k^*(n), \quad (7)$$

when $l = 1$, Eq. (7) degenerates into WGRFT [34]; when $\alpha = 1$, Eq. (7) degenerates into MWGFT [25]; when $l = \alpha = 1$, Eq. (7) degenerates into WGFT [17].

Proposition 1. (Diagonal clustering of the vertex-frequency representation with fractional order $\alpha \rightarrow 0$) When α tends to 0, the vertex-frequency representation of MWGFRFT is clustered on the main diagonal, i.e., all values outside the main diagonal equal to 0.

Proof. See Appendix D. \square

Note that Proposition 1 is also true for FMWGRFT, MWGFT [25], WGRFT [34] and WGFT [17] and so on.

IV. FAST MULTI-WINDOWED GRAPH FRACTIONAL FOURIER TRANSFORM

To improve computational speed, we introduce a fast multi-windowed graph fractional Fourier transform (FMWGRFT) algorithm. In the classic scenario of signals, the windowed Fourier transform can be calculated through an inverse Fourier transform from the ‘ α -domain’ (the Fourier transform of the windowed Fourier domain) [36]. Applying the idea to graphs [34], we define the G^α -domain as the SGFRFT of MWGFRFT in graph fractional Fourier domain:

$$G^\alpha(k, k') = \sum_{l=1}^L \sum_{i=1}^N Wf(\mathbf{g}_{i,k'}^{(l\alpha)}) \gamma_k^*(i). \quad (8)$$

Applying (7) to (8), similar to [34], then we get

$$G^\alpha(k, k') = N^\alpha \tilde{f}(k, k') \hat{\mathbf{g}}_{l\alpha}^*(r_k),$$

where $\tilde{f}(k, k') = \sum_{d=1}^N f(d) \gamma_k^*(d) \gamma_k^*(d)$.

Definition 6. (Fast multi-windowed graph fractional Fourier transform). The inverse SGFRFT of G^α on the variable k is FMWGRFT, i.e.,

$$FWf(\mathbf{g}_{i,k'}^{(l\alpha)}) = \sum_{l=1}^L \sum_{k=0}^{N-1} N^\alpha \tilde{f}(k, k') \hat{\mathbf{g}}_{l\alpha}^*(r_k) \gamma_k(i).$$

The calculation algorithm of FMWGRFT is defined as follows:

(i) The loop about $\hat{\mathbf{g}}_{l\alpha}$ for $l = 1, \dots, L$. This step has $O(L)$ computational complexity.

(ii) Calculate $\tilde{f}(k, k')$ by using matrices:

$$\tilde{F} = [\tilde{f}(k, k')] = (F \circ \gamma^H) * \gamma,$$

where \circ represents Hadamard multiplication and $*$ denotes the standard matrix multiplication. Each row of F is the signal \mathbf{f} , and γ^H denotes the complex conjugate of the graph fractional basis γ . This step has $O(N^3)$ computational complexity.

(iii) Form a matrix such that each row is the SGFRFT of a window function \mathbf{g}_l .

$$\Psi^{l\alpha} = \begin{pmatrix} \hat{\mathbf{g}}_{l\alpha}(r_0) & \hat{\mathbf{g}}_{l\alpha}(r_1) & \cdots & \hat{\mathbf{g}}_{l\alpha}(r_{N-1}) \\ \hat{\mathbf{g}}_{l\alpha}(r_0) & \hat{\mathbf{g}}_{l\alpha}(r_1) & \cdots & \hat{\mathbf{g}}_{l\alpha}(r_{N-1}) \\ \vdots & \vdots & \ddots & \vdots \\ \hat{\mathbf{g}}_{l\alpha}(r_0) & \hat{\mathbf{g}}_{l\alpha}(r_1) & \cdots & \hat{\mathbf{g}}_{l\alpha}(r_{N-1}) \end{pmatrix}$$

This step does not influence the computational complexity.

(iv) Calculate the G^α -domain representation.

$$G^\alpha = N^\alpha * (\Psi^{l\alpha})^* \circ \tilde{F}.$$

The computational complexity is $O(N^2)$.

(v) The vertex-frequency content is obtained by applying inverse SGFRFT to each row of G^α , i.e.

$$FWf(l) = \gamma * (G^\alpha)^T,$$

where $(G^\alpha)^T$ denotes the non-conjugate transpose of G^α . The complexity of this step is $O(N^3)$.

(vi) Perform matrix addition on these L matrices. The complexity of this step is $O(LN^2)$.

To sum up, the computational complexity of FMWGRFT is $O(LN^3)$. As N increases, this computational complexity is a significant improvement, compared with MWGFRFT algorithm and MWGFT [25] algorithm which have the computational complexity of $O(LN^4)$.

V. DUAL OF MULTI-WINDOWED GRAPH FRACTIONAL FOURIER FRAMES

In this section, we obtain a reconstruction formula by introducing the dual of multi-windowed graph fractional Fourier frames. In addition, the canonical dual is also introduced.

Let $\tilde{\mathcal{G}}_{l\alpha}^w$ denote the set of multi-windowed graph fractional Fourier atoms, generated by a finite sequence of window functions $\tilde{\mathbf{g}}_1, \tilde{\mathbf{g}}_2, \dots, \tilde{\mathbf{g}}_N$ in the sense of (3). $\tilde{\mathcal{G}}_{l\alpha}^w$ is called a dual to $\mathcal{G}_{l\alpha}^w$ if for any $\mathbf{f} \in \mathbb{C}^N$, there exists a constant C such that

$$\begin{aligned} \mathbf{f} &= C \sum_{l=1}^L \sum_{k=0}^{N-1} \sum_{i=1}^N \langle \mathbf{f}, \tilde{\mathbf{g}}_{i,k}^{(l\alpha)} \rangle \mathbf{g}_{i,k}^{(l\alpha)} \\ &= C \sum_{l=1}^L \sum_{k=0}^{N-1} \sum_{i=1}^N \langle \mathbf{f}, \mathbf{g}_{i,k}^{(l\alpha)} \rangle \tilde{\mathbf{g}}_{i,k}^{(l\alpha)}. \end{aligned} \quad (9)$$

Theorem 2. Suppose that $\mathcal{G}_{l\alpha}^w$ is a multi-windowed graph fractional Fourier frame as defined in (3). If there exists a finite sequence of window functions $\tilde{\mathbf{g}}_1, \tilde{\mathbf{g}}_2, \dots, \tilde{\mathbf{g}}_L$ and a constant $\mu > 0$ such that

$$\sum_{l=1}^L \hat{\mathbf{g}}_{l\alpha}^*(r_p) \hat{\mathbf{g}}_{l\alpha}(r_p) = \mu, \quad p = 0, 1, \dots, N-1,$$

then $\tilde{\mathcal{G}}_{l\alpha}^w$ is a dual of $\mathcal{G}_{l\alpha}^w$.

Proof. See Appendix E. \square

We could also prove that the dual $\tilde{\mathcal{G}}_{l\alpha}^w$ of a multi-windowed graph fractional Fourier frame $\mathcal{G}_{l\alpha}^w$ is also a frame.

Corollary 3. *Suppose that $\mathcal{G}_{l\alpha}^w$ is a multi-windowed graph fractional Fourier frame as defined in (3). If there exists a finite sequence of window functions $\tilde{\mathbf{g}}_1, \tilde{\mathbf{g}}_2, \dots, \tilde{\mathbf{g}}_L$ and a constant $\mu > 0$ such that $\sum_{l=1}^L \tilde{\mathbf{g}}_{l\alpha}^*(r_p) \tilde{\mathbf{g}}_{l\alpha}(r_p) = \mu$ for $p = 0, 1, \dots, N-1$, then $\tilde{\mathcal{G}}_{l\alpha}^w$ is also a multi-windowed graph fractional Fourier frame.*

Proof. See Appendix F. \square

Corollary 4. *Suppose that $\mathcal{G}_{l\alpha}^w$ is a multi-windowed graph fractional Fourier frame as defined in (3). Let $\mathbf{c} \in \mathbb{C}^N$ be a vector with $c_n = N^\alpha \sum_{l=1}^L \|T_n^\alpha \mathbf{g}_l\|_2^2$ and $\mathbf{d} \in \mathbb{C}^N$ be a vector with $d_n = \frac{1}{c_n}$ for $n = 1, 2, \dots, N$. Then the canonical dual frame of $\tilde{\mathcal{G}}_{l\alpha}^w$ is given by*

$$\tilde{\mathcal{G}}_{l\alpha}^w := \{\tilde{\mathbf{g}}_{i,k}^{(l\alpha)} = \mathbf{d} \circ \mathbf{g}_{i,k}^{(l\alpha)}\},$$

where $i = 1, 2, \dots, N$; $k = 0, 1, \dots, N-1$; $l = 1, 2, \dots, L$; $0 < \alpha \leq 1$.

Proof. See Appendix G. \square

VI. SHIFT MULTI-WINDOWED GRAPH FRACTIONAL FOURIER FRAMES

In GSP, the adjacency matrix acts as a shift operator [1]. In graph fractional Fourier domain, different fractional shift operators are proposed [37], [38], [39]. Assume that the eigen-decomposition of the graph adjacency matrix is $\mathbf{A} = VJV^{-1}$, in this paper, define the graph fractional shift operator as

$$S^\alpha = VJ^\alpha V^{-1},$$

to facilitate the construction of tight frames in Section VII later. Then we could design a new type of frames and introduce the concept of shift multi-windowed graph fractional Fourier transform (SMWGFRFT).

Theorem 3. *Given L window vectors $\mathbf{g}_l \in \mathbb{C}^N$ with $S^\alpha \mathbf{g}_l \neq 0$ for $l = 1, \dots, L$. Define $\mathbf{g}_{i,l} := \gamma_i \circ (S^\alpha \mathbf{g}_l)$, where \circ denotes the Hadamard product. Also define*

$$\mathbf{c} = (c_1, c_2, \dots, c_N)^T, \text{ with } c_k = \tilde{\mathbf{s}}_k \mathbf{G} \tilde{\mathbf{s}}_k^*, \quad (10)$$

where $\tilde{\mathbf{s}}_k$ is the k th row of matrix S^α and $\mathbf{G} = \sum_{i=1}^L \mathbf{g}_i \mathbf{g}_i^*$. The set of shift multi-window graph fractional Fourier atoms

$$\mathcal{G}_{l\alpha}^s := \{\mathbf{g}_{i,l}\}_{i=0,1,\dots,N-1;l=1,2,\dots,L} \quad (11)$$

forms a frame (i.e., SMWGFRFF) for signals defined on \mathcal{G} if and only if $c_k > 0$ for all of elements of \mathbf{c} . The optimal lower and upper frame bounds are

$$A = \min_{k \in \{1,2,\dots,N\}} c_k \text{ and } B = \max_{k \in \{1,2,\dots,N\}} c_k, \quad (12)$$

respectively.

Proof. See Appendix H. \square

Corollary 5. *Suppose that $\mathcal{G}_{l\alpha}^s$ is a shift multi-windowed graph fractional Fourier frame as defined in (11). Let $\mathbf{c} \in \mathbb{C}^N$ be a vector with $c_k = \tilde{\mathbf{s}}_k \mathbf{G} \tilde{\mathbf{s}}_k^*$ and $\mathbf{d} \in \mathbb{C}^N$ be a vector with $d_n = \frac{1}{c_n}$ for $n = 1, 2, \dots, N$. Then the canonical dual frame of $\mathcal{G}_{l\alpha}^s$ is defined as $\tilde{\mathcal{G}}_{l\alpha}^s = \{\tilde{\mathbf{g}}_{i,l} = \mathbf{d} \circ \mathbf{g}_{i,l}\}$, where $n = 1, 2, \dots, N$; $i = 0, 1, \dots, N-1$; $l = 1, 2, \dots, L$.*

Proof. The proof is similar to Corollary 4. \square

Corollary 6. *Let $\mathcal{G}_{l\alpha}^s$ be a shift multi-windowed graph fractional Fourier frame and $\tilde{\mathbf{s}}_k$ is the k th row of matrix S^α . $\mathcal{G}_{l\alpha}^s$ is a tight frame if and only if $\tilde{\mathbf{s}}_k \mathbf{G} \tilde{\mathbf{s}}_k^* = C$ for $k = 1, \dots, N$, where C is a constant number and $\mathbf{G} = \sum_{i=1}^L \mathbf{g}_i \mathbf{g}_i^*$.*

Proof. See Appendix I. \square

It is known that $S^\alpha = \begin{pmatrix} \tilde{\mathbf{s}}_1 \\ \vdots \\ \tilde{\mathbf{s}}_N \end{pmatrix}$, where $\tilde{\mathbf{s}}_i$ is the i th row of

matrix S^α . Then we define $S_i^\alpha = (\tilde{\mathbf{s}}_i)^T$, where $(\tilde{\mathbf{s}}_i)^T$ denotes the non-conjugate transpose of $\tilde{\mathbf{s}}_i$. Given window functions $\mathbf{g}_1, \dots, \mathbf{g}_L \in \mathbb{C}^N$, we can define a new set of shift multi-windowed graph fractional Fourier atoms by

$$\mathcal{G}_{l\alpha}^{sw} = \{\mathbf{g}_{i,k}^{(l\alpha)}\}_{i=1,2,\dots,N;k=0,1,\dots,N-1;l=1,2,\dots,L;0 < \alpha \leq 1}, \quad (13)$$

where

$$\mathbf{g}_{i,k}^{(l\alpha)}(n) = (M_k^\alpha S_i^\alpha \mathbf{g}_l)(n).$$

Definition 7. (Shift multi-windowed graph fractional Fourier transform) *Given window functions $\mathbf{g}_1, \dots, \mathbf{g}_L \in \mathbb{C}^N$, let $\mathcal{G}_{l\alpha}^{sw}$ is a shift multi-windowed graph fractional Fourier frame defined in (13). For a graph signal $\mathbf{f} \in \mathbb{C}^N$, the SMWGFRFT of \mathbf{f} is denoted by*

$$SWf(\mathbf{g}_{i,k}^{(l\alpha)}) := \langle \mathbf{f}, \mathbf{g}_{i,k}^{(l\alpha)}(n) \rangle.$$

It is apparently that the computational complexity of SMWGFRFT is $O(LN^3)$.

VII. TWO TYPES OF TIGHT MULTI-WINDOWED GRAPH FRACTIONAL FOURIER FRAMES

In this section, we design tight multi-windowed graph fractional Fourier frames (TMWGFRFF) and tight shift multi-windowed graph fractional Fourier frames (TSMWGFRFF).

A. Construction of TMWGFRFF

Constructing tight MWGFRFF is equivalent to find L window functions $\{\mathbf{g}_1, \mathbf{g}_2, \dots, \mathbf{g}_L\}$ such that $\sum_{l=1}^L \|T_n^\alpha \mathbf{g}_l\|_2^2 = C$ for $n = 1, 2, \dots, N$. By Corollary 2, the goal of the construction is to find a sequence of window functions such that $\sum_{l=1}^L |\tilde{\mathbf{g}}_{l\alpha}(r_p)|^2 = 1$ for $r_p \in R$, where R denotes graph fractional Laplacian spectrum. Among the functions with such a property, we think of the cardinal B-spline as a candidate.

The k th order cardinal B-spline \mathbf{N}_k is defined as follows:

$$\mathbf{N}_k(x) = \int_0^1 \mathbf{N}_{k-1}(x-t) dt.$$

The integer-translates of the k th order cardinal B-spline form a partition of unity, i.e.,

$$\sum_{p \in \mathbb{Z}} \mathbf{N}_k(x - p) = 1, \forall k \in \mathbb{N}^+. \quad (14)$$

Suppose that the normalized graph fractional Laplacian matrix is applied, that is, the corresponding graph fractional Laplacian spectrum is contained in $[0, 2]$. We then take B-spline \mathbf{N}_2 to construct the tight frame window functions:

$$\mathbf{N}_2(x) = \begin{cases} x, & x \in [0, 1), \\ 2 - x, & x \in [1, 2], \\ 0, & \text{else.} \end{cases}$$

Letting $|\hat{g}_{1\alpha}|^2 = \mathbf{N}_2(x - 1)$, $|\hat{g}_{2\alpha}|^2 = \mathbf{N}_2(x)$, and $|\hat{g}_{3\alpha}|^2 = \mathbf{N}_2(x + 1)$, according to Eq. (14), we have $\sum_{l=1}^3 |\hat{g}_{l\alpha}(\lambda_p)|^2 = 1$, $\lambda_p \in [0, 2]$. That is, $\{g_1, g_2, g_3\}$ is a set of tight frame window functions.

B. Construction of TSMWGRFF

When the rows of the graph fractional shift operator S^α have identical 2-norm, we could construct orthonormal vectors as the tight SMWGRFF:

(i) the graph fractional Laplacian eigenvectors, i.e. $\mathbf{g}_l = \gamma_{l-1}$ for $l = 1, 2, \dots, N$, where γ_l is the l th eigenvector of the graph fractional Laplacian matrix.

(ii) Householder vectors with localized generator, i.e. $\mathbf{g}_l = \mathbf{h}_l$, where \mathbf{h}_l is the l th vector of the Householder matrix $\mathbf{H} = \mathbf{I}_N - 2\mathbf{v}\mathbf{v}^T$ and \mathbf{v} is a vector localized on a small set of indices.

VIII. EXPERIMENTS

We conduct several simulations by using frame, dual frame, and tight frame window functions to evaluate the effectiveness of MWGRFT, FMWGRFT, and SMWGRFT in extracting the vertex-frequency features of graph signals. Our methods are also compared with WGFT[17], MWGFT[25] and WGRFT[34].

A. Comparative Analysis of Vertex-Frequency Feature Extraction among WGFT[17], MWGFT[25], WGRFT[34] and FMWGRFT

First, we consider a path graph with 256 vertices, all of which have equal weights of 1. The eigenvectors of the graph Laplacian are generated from the basis vectors of the DCT-II transform. We consider the following three signals in Fig. 2: f_1 is a band limited signal in graph fractional Fourier domain, f_2 and f_3 are bandpass signals in graph fractional Fourier domain. We choose the heat diffusion kernel as the window function by setting $\hat{g}_\alpha(\lambda_\ell) = Ce^{-\tau\lambda_\ell}$ with $\tau = 300$ and choosing C such that $\|\hat{g}_\alpha\|_2 = 1$. Applying Eq.(1) to \hat{g}_α , then obtain $L = 10$ windows. The ‘‘spectrograms’’ in Fig. 3 show $|Wf|^2$ for all $i \in \{1, 2, \dots, 256\}$ and $k \in \{0, 1, \dots, 255\}$.

From Fig. 3, the vertex-frequency features of the three signals are clearly observed using MWGRFT, enabling precise identification of the brightest points by combining their vertex and frequency information. However, none of WGFT,

MWGFT and WGRFT can accurately extract the vertex-frequency features of the three signals. The vertex domain features of the three signals by WGFT are unclear and cannot be accurately determined. For MWGFT, the vertex domain features of the 3 signals are clearly determined, however, the corresponding frequency features at each vertex cannot be accurately localized, nor can the location of the brightest point in the spectrograms be determined. For WGRFT, no accurate vertex features are identified, and all frequency features are located at the smallest vertices i .

B. Algorithm evaluation of FMWGRFT

To evaluate the performance of FMWGRFT algorithm, we conducted experiments to demonstrate its effectiveness and robustness.

(i) effectiveness

To clearly demonstrate the temporal advantage of the fast algorithm, we compare the time cost of the fast algorithm (FMWGRFT) with the original algorithm (MWGRFT). Setting the fractional order $\alpha = 0.8$, we contemplate a random ring graph with different number of vertices N , where the signal is $f_5(n)$. We choose the standard Gaussian function as the window function \hat{g}_α , applying Eq.(1) to \hat{g}_α , and then obtain $L = 10$ windows. In Fig. 4, the x-axis represents the logarithm of the number of vertices and the y-axis represents the logarithm of computation time (in seconds). For MWGRFT, the red line corresponds to a linear fit, aligning with the theoretical computational complexity of $O(LN^4)$. Similarly, for FMWGRFT, the blue line corresponds to a linear fit, which matches the theoretical computational complexity of $O(LN^3)$. The results indicate that FMWGRFT is more efficient and requires less computation time compared to MWGRFT.

(ii) Robustness

In the first experiment, we simulate with 3 graphs of 200 vertices: a ring graph, a random ring graph and a sphere graph. We take the real parts of the 3 graph signals as follows.

$$\begin{aligned} f_4(n) &= Re(\gamma_{100}^r(n)), \\ f_5(n) &= Re(\gamma_{50}^\pi(n) + \gamma_{90}^\pi(n) + \gamma_{150}^\pi(n)), \\ f_6(n) &= Re(\gamma_{64}^s(n) + \gamma_{128}^s(n)). \end{aligned}$$

For fixed $\alpha = 0.95$, we take $f_4(n)$, $f_5(n)$ and $f_6(n)$ from the fractional Laplacian matrix of a ring graph, a random ring graph and a sphere graph, respectively. The details of the original signals are shown in Fig. 5(a),(d),(g). We choose the heat diffusion kernel as the window function \hat{g}_α . In Fig. 5, we note that the details of the spectrograms by MWGRFT and FMWGRFT are the same. Moreover, we can observe that the vertex-frequency representations of FMWGRFT closely match that of MWGRFT for the 3 signals; moreover, FMWGRFT effectively identified the correct frequencies, further validating the correctness and effectiveness of FMWGRFT algorithm.

In the second experiment, we vary both the fractional order and the noise parameter. The normalized mean squared error (NMSE) is computed between the FMWGRFT coefficients of 3 original signals and their corresponding contaminated signals, as illustrated in Fig. 6. In Fig. 7, the WGRFT results

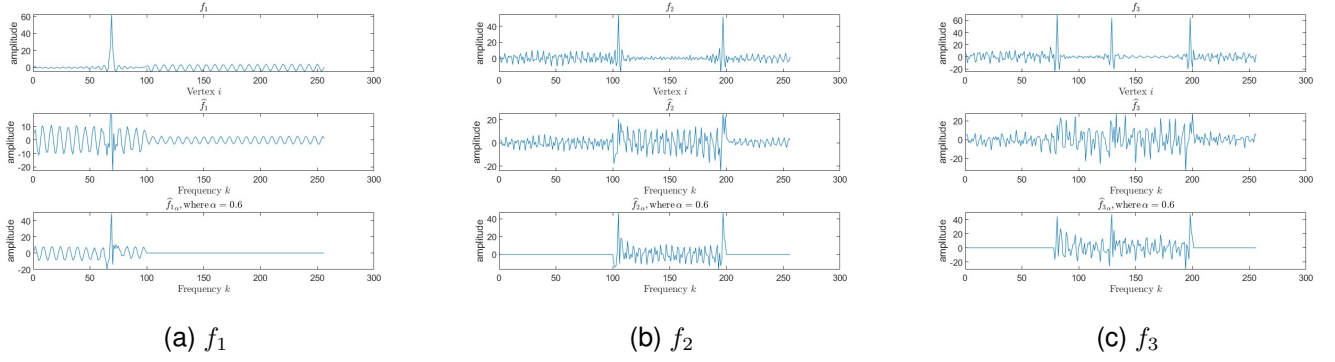


Fig. 2. The signal f_1 , f_2 , and f_3 .

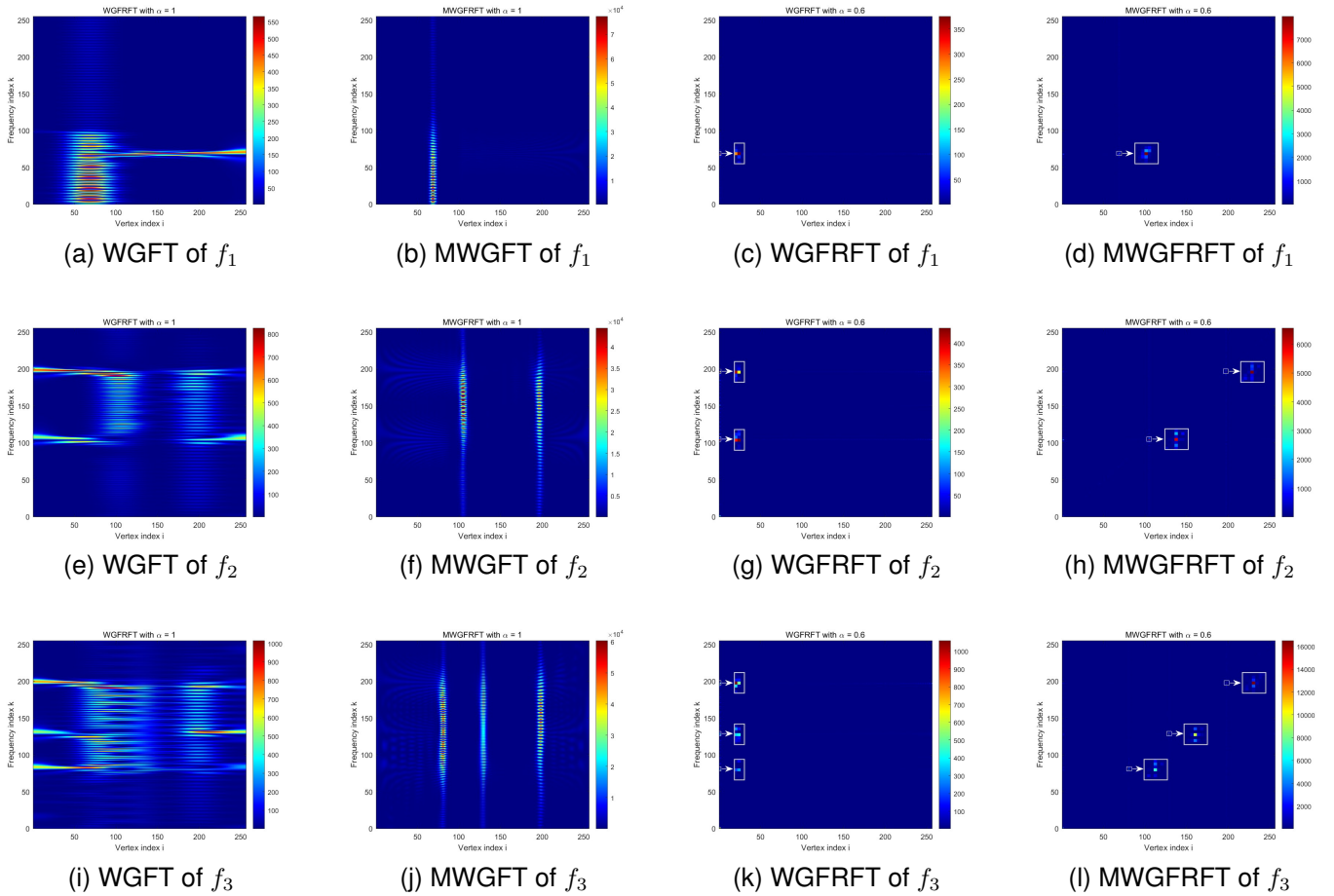


Fig. 3. Vertex-frequency representations of signals f_1 , f_2 , and f_3 by WGFT, MWGFT, WGRFT and MWGRFT, with fractional order $\alpha = 0.6$ (Observe the six spectrograms (c-d), (g-h), and (k-l), where each larger rectangular box, marked by an arrow, presents a magnified view of the corresponding smaller rectangular box within the spectrogram).

are presented by using a single window function, while all other conditions remain identical to those in Fig. 6. respectively.

We experiment with 3 graphs of $N = 300$ vertices: for the sphere graph, we add Poisson noise with parameter $\lambda = 0.2, 0.3$, and 0.5 to signal f_7 ; for the community graph, we add exponential noise with parameter $\lambda = 0.2, 0.3$, and 0.5 to signal f_8 ; for the swiss roll graph, we add Gaussian noise with standard deviation $\sigma = 0.2, 0.3$, and 0.5 to signal f_9 ,

$$f_7(n) = \sin(110\pi n/N), \text{ for } 1 \leq n \leq 300$$

$$f_8(n) = \begin{cases} \sin(160\pi n/N), & \text{for } 1 \leq n \leq 90 \\ \sin(70\pi n/N), & \text{for } 91 \leq n \leq 170 \\ \sin(200\pi n/N), & \text{for } 171 \leq n \leq 300 \end{cases}$$

$$f_9(n) = \sin\left(\left(30n + \frac{1}{5}n^2\right)\pi/N\right), \text{ for } 1 \leq n \leq 300$$

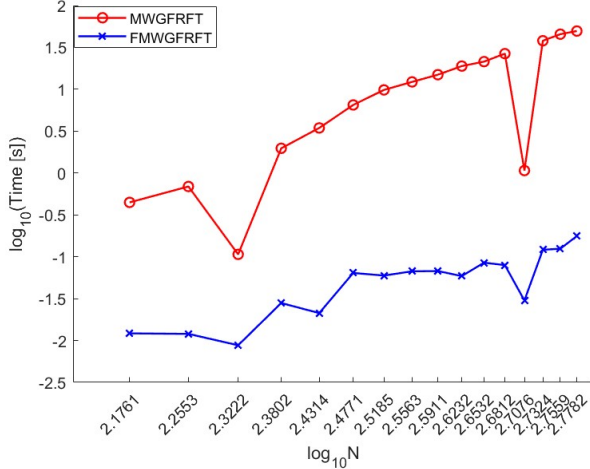


Fig. 4. Time cost comparison of MWGFRFT and FMWGRFT

For the original signals f_7, f_8 and f_9 , the contaminated signals are denoted by \bar{f}_7, \bar{f}_8 and \bar{f}_9 . We choose the standard Gaussian function as the window function by setting $\hat{g}_\alpha(\lambda_\ell) = Ce^{-\tau\lambda_\ell^2}$ with $\tau = 0.5$ and choosing C such that $\|\hat{g}_\alpha\|_2 = 1$. Applying Eq. (1) to \hat{g}_α , and then obtain $L = 20$ windows. We then calculate the normalized mean squared error (NMSE) between the transform coefficients of the original signal and the contaminated signal, which is given by:

$$\text{NMSE} = \frac{\text{MSE}}{\|FWf\|_2^2},$$

where $\text{MSE} = \frac{1}{N^2} \sum_{i=1}^N \sum_{k=0}^{N-1} (FWf - FW\bar{f})^2$, N is the number of vertices, FWf and $FW\bar{f}$ are the FWGRFT coefficients of the original and contaminated signals, respectively.

From Fig. 6 and Fig. 7, we observe that, despite differences in graph structure and noise, a higher noise parameter corresponds to a larger value of NMSE. Compared to WGFT, MWGFT and WGRFT, the FMWGRFT algorithm consistently achieves the lower NMSE, highlighting its robustness and reliability across diverse scenarios. To minimize the value of NMSE, an appropriate choice of fractional order α can be chosen depending on the specific case.

C. Examples of SMWGRFT and FMWGRFT

First, we analyze two distinct graph structures: a ring graph with 60 vertices paired with the signal f_{10} , and a Swiss roll graph with 60 vertices paired with the signal f_{11} . We choose the heat diffusion kernel as the window function by setting $\hat{g}_\alpha(\lambda_\ell) = Ce^{-\tau\lambda_\ell}$ with $\tau = 60$ and choosing C such that $\|\hat{g}_\alpha\|_2 = 1$. Applying Eq.(1) to \hat{g}_α , and then obtain $L = 10$ windows. From Fig. 8, we know that SMWGRFT fails to identify vertex or frequency information, overlooking key vertex-frequency features. Comparing Fig. 8(c) and Fig. 8(d), we observe that FMWGRFT effectively identifies vertex-frequency features. In contrast, while SMWGRFT demonstrates proficiency in capturing vertex-frequency features, it misidentifies certain vertices. By comparing Fig. 8(g)

with Fig. 8(h), we observe that FMWGRFT identifies only the prominent vertex-frequency features, disregarding those with less distinct features. In contrast, SMWGRFT captures all vertex-frequency features but introduces some errors in identifying certain points. Therefore, SMWGRFT and FMWGRFT can complement each other in identifying vertex-frequency features and are best utilized in combination.

Second, we analyze a community graph with 80 vertices and the signal f_{12} . We choose the dual heat diffusion kernel as the window function by setting $\hat{g}_\alpha(\lambda_\ell) = \frac{\mu}{e^{-\tau\lambda_\ell}}$ with $\tau = 60$ and $\mu > 0$, choosing μ such that $\|\hat{g}_\alpha\|_2 = 1$. Applying Eq.(1) to \hat{g}_α , and then obtain L windows. In Fig. 9, the spectrograms are generated by using dual FMWGRFT and dual SMWGRFT with $\alpha = 0.6$. Fig. 9 demonstrates that both dual FMWGRFT and dual SMWGRFT are capable of extracting vertex-frequency features.

Thirdly, we consider a random ring graph with 50 vertices and the signal f_{13} in Fig. 10. The FMWGRFT window functions is derived from B-spline N_2 by Section VII-A. The SMWGRFT window functions is given by the Householder matrix. By Section VII-B(ii), the Householder matrix \mathbf{H} is obtained, where

$$\mathbf{v}(n) = \begin{cases} e^{-0.5(n-1)} & 1 \leq n \leq 10, \\ 0 & n \geq 11. \end{cases}$$

Fig. 10 demonstrates that both tight FMWGRFT and Householder tight SMWGRFT are capable of extracting vertex-frequency features.

IX. APPLICATIONS: ANOMALY DETECTION

In graph fractional Fourier domain, WGFT [17], MWGFT [25], WGRFT [34], SMWGRFT and FMWGRFT are applied to detect anomaly signals. The test involves an anomaly signal f_{14} in Fig.11(a), characterized by two anomalous deep red vertices, on a community graph with 20 vertices. The spectrograms are computed by using WGFT [17], MWGFT [25], WGRFT [34], SMWGRFT, SMWGRFT and FMWGRFT. Taking maximum of \mathbf{S} with respect to the vertices, the spectrogram coefficient threshold is defined as $\delta = \frac{1}{2} \max(\mathbf{S})$, where \mathbf{S} represents the spectrogram coefficient. Vertices with maximum spectrogram coefficients exceeding δ are highlighted in red. In Fig.11(b), the WGFT spectrogram detects all vertices as anomalies. In Fig.11(c), the MWGFT spectrogram identifies all anomalous vertices but incorrectly classifies one additional vertex as anomalous. In Fig. 11(d), the WGRFT spectrogram fails to detect the anomalous vertices. In Fig.11(e), the SMWGRFT spectrogram also fails to detect the anomalous vertices. In Fig.11(f), the SMWGRFT spectrogram identifies one anomaly vertex but incorrectly classifies too many vertices as anomalous. In Fig. 11(g), the FMWGRFT spectrogram successfully detects all anomalous vertices. This example highlights the effectiveness of FMWGRFT in accurately identifying the vertices associated with the anomaly signals.

X. CONCLUSION

By performing a comparative analysis of vertex-frequency feature extraction among WGFT [17], WGRFT [34],

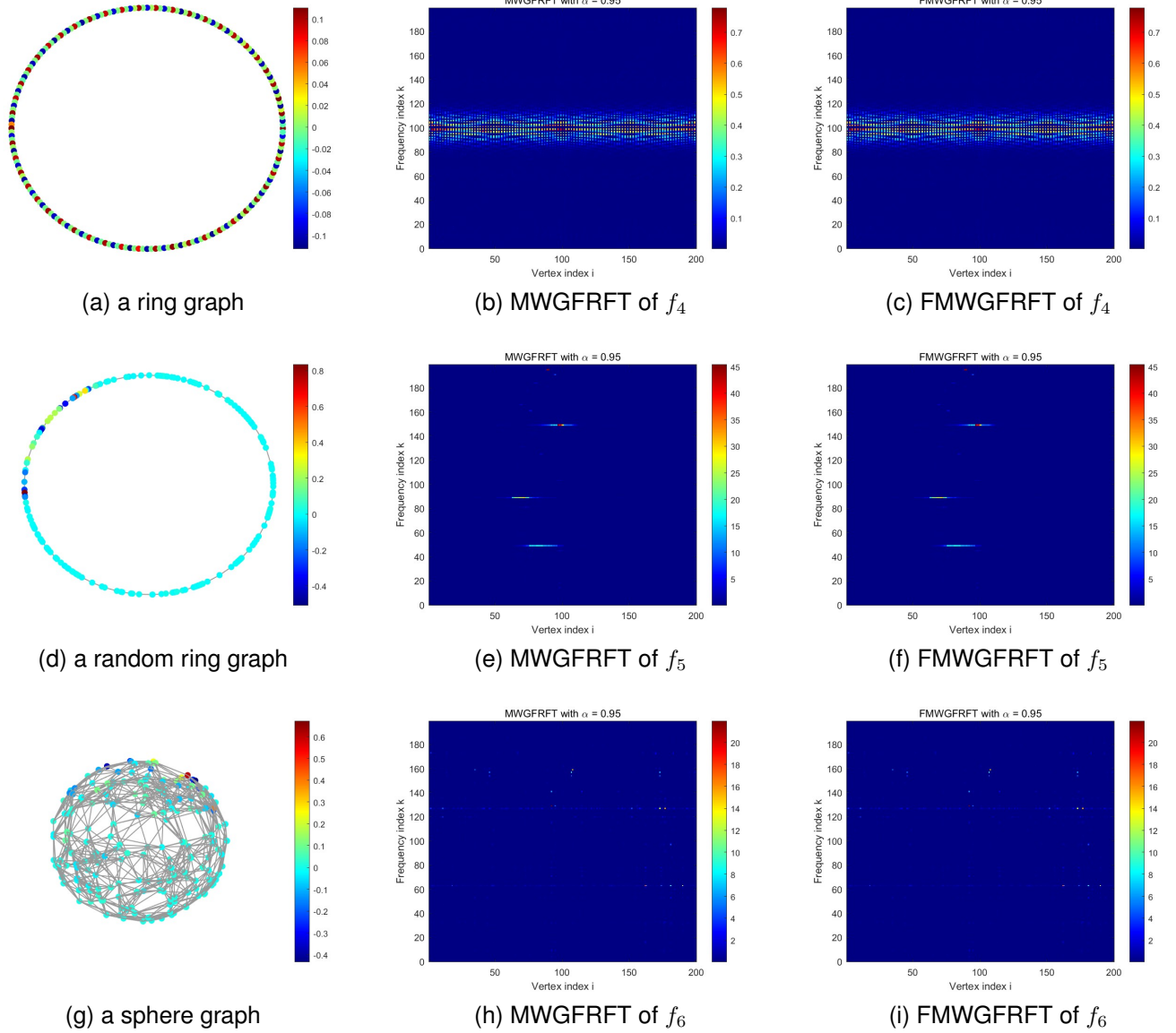


Fig. 5. Vertex-frequency representations of signals f_4 , f_5 , and f_6 by MWGFRFT and FMWGRFT, with $\alpha = 0.95$.

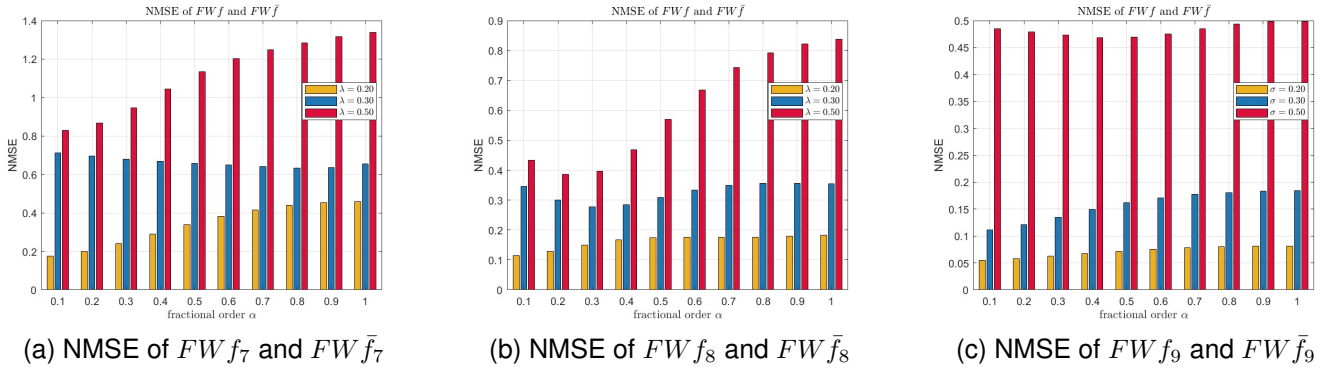


Fig. 6. NMSE of FWf and $FW\bar{f}$ for f_7 , f_8 , and f_9 by FMWGRFT with different fractional order α . (It is MWGFT[25] for $\alpha = 1$)

MWGFT [25], and MWGFRFT, it becomes evident that representation in the graph fractional Fourier domain for MWGFRFT offers significant advantages in vertex-frequency given window functions. The performance of MWGFRFT and

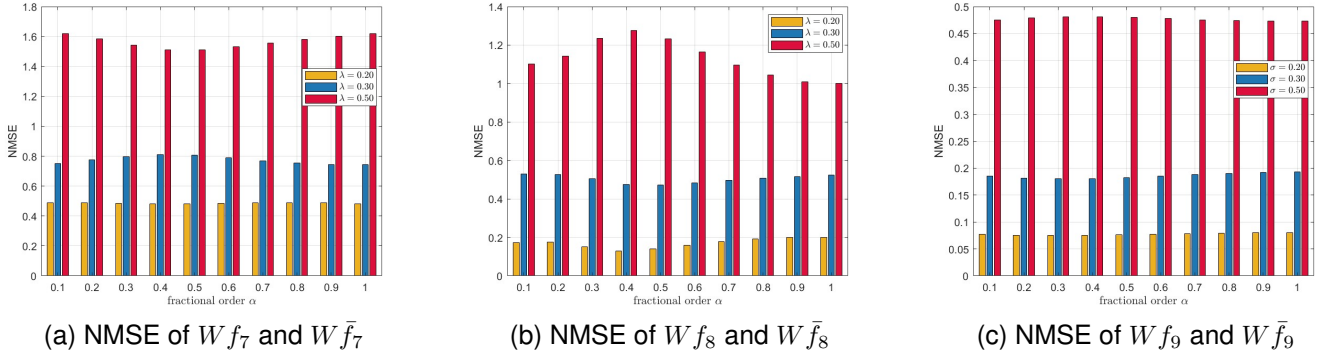


Fig. 7. NMSE of Wf and $\bar{W}\bar{f}$ for f_7 , f_8 , and f_9 by WGRFT [34] with different fractional order α . (It is WGFT[17] for $\alpha = 1$)

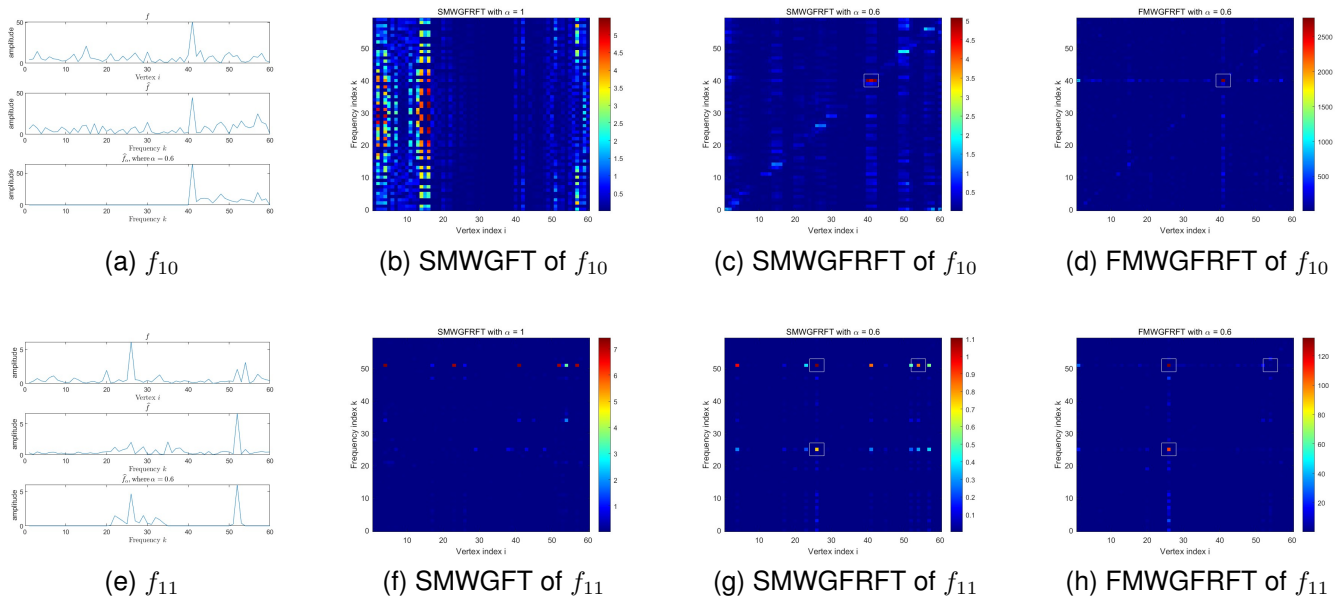


Fig. 8. Vertex-frequency representations of signals f_{10} and f_{11} by SMWGFT, SMWGRFT and FMWGRFT with fractional order $\alpha = 0.6$.

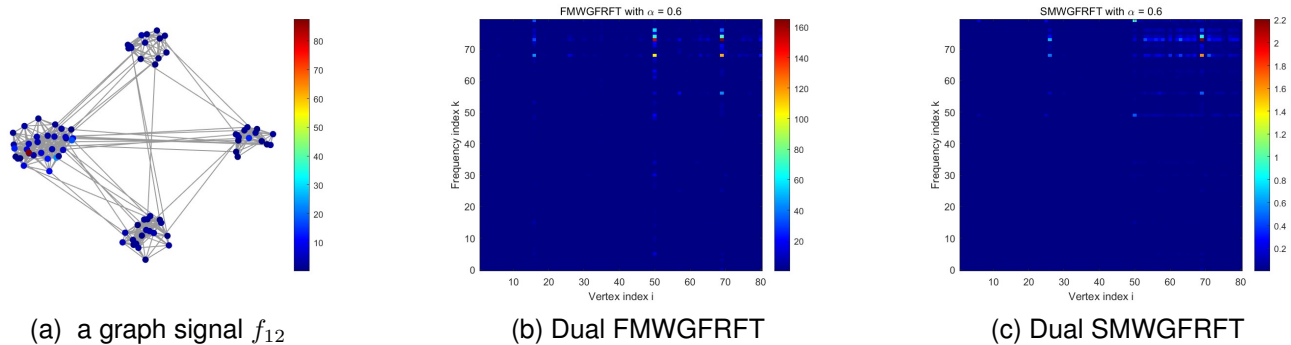


Fig. 9. The spectrograms generated by dual FMWGRFT and dual SMWGRFT with $\alpha = 0.6$.

FMWGRFT is compared with regard to vertex-frequency representation, normalized mean squared error, and time cost. The experimental results demonstrate the robustness and effectiveness of the FMWGRFF algorithm. Experiments with SMWGRFT and FMWGRFT on different graphs demonstrate that SMWGRFT and FMWGRFT effectively ex-

tract vertex-frequency features. Furthermore, SMWGRFT and FMWGRFT are mutually complementary in identifying vertex-frequency features and are most effective when utilized in tandem. Additionally, dual and tight frame window functions have demonstrated effectiveness in extracting vertex-frequency features. In the graph fractional domain,

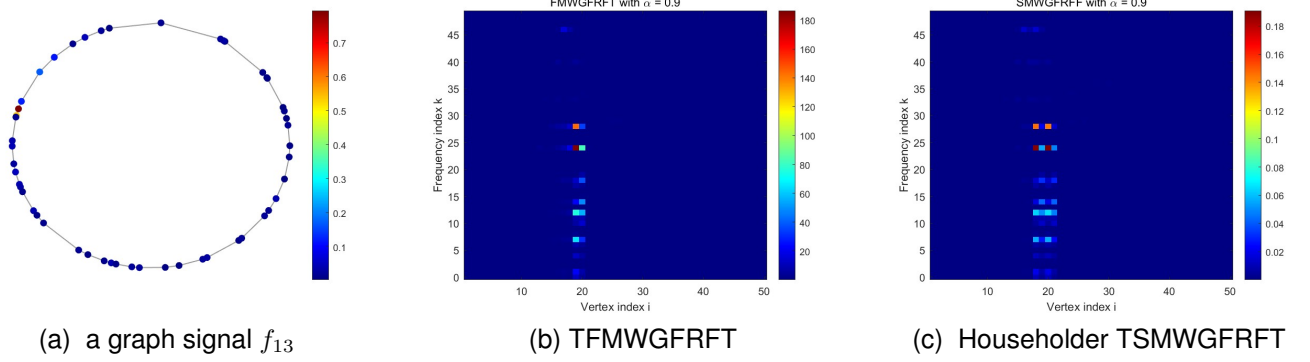


Fig. 10. The spectrograms generated by tight FMWGRFT and Householder tight SMWGRFT with $\alpha = 0.9$.

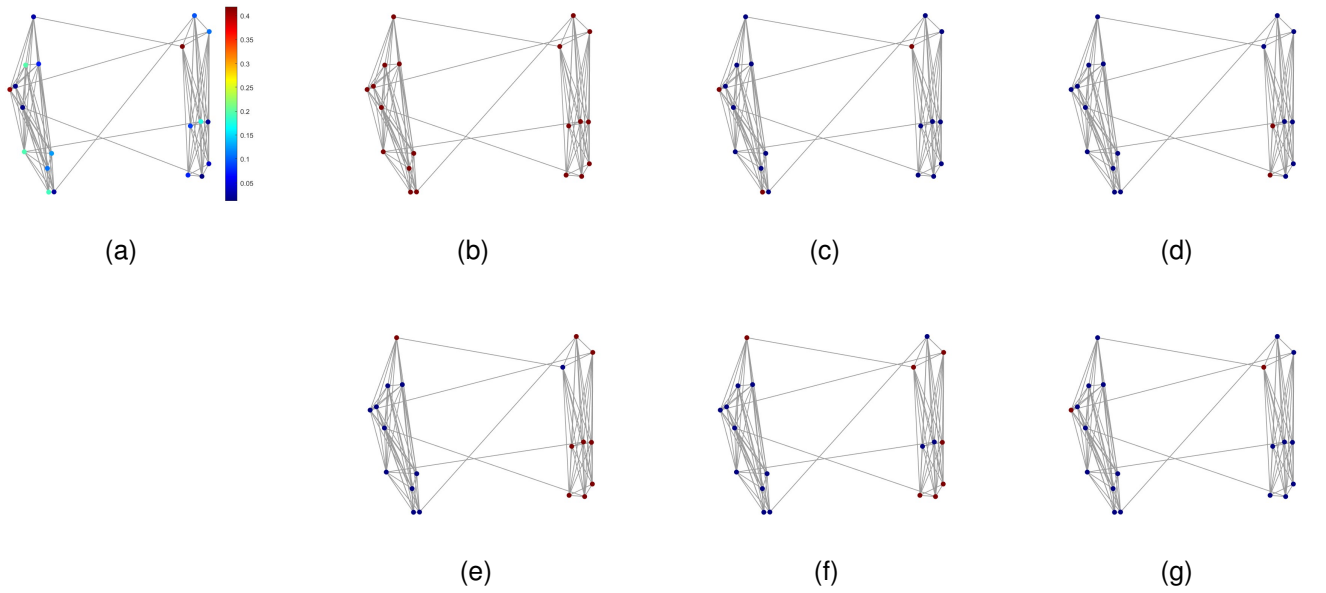


Fig. 11. (a) An anomaly signal f_{14} ; (b) Anomaly vertices detected by the WGFT spectrogram on f_{14} ; (c) Anomaly vertices detected by the MWGFT spectrogram on f_{14} ; (d) Anomaly vertices detected by the WGRFT spectrogram on f_{14} ; (e) Anomaly vertices detected by the SMWGFT spectrogram on f_{14} ; (f) Anomaly vertices detected by the SMWGRFT spectrogram on f_{14} ; (g) Anomaly vertices detected by the FMWGRFT spectrogram on f_{14} (fractional order $\alpha = 0.6$).

FMWGRFT demonstrates effectiveness in accurately detecting anomaly signals.

APPENDIX A
PROOF OF THEOREM 1

For any $\mathbf{f} \in \mathbb{C}^N$,

$$\begin{aligned}
 & \sum_{l=1}^L \sum_{i=1}^N \sum_{k=0}^{N-1} |\langle \mathbf{f}, \mathbf{g}_{i,k}^{(l\alpha)} \rangle|^2 \\
 &= N^\alpha \sum_{l=1}^L \sum_{i=1}^N \sum_{k=0}^{N-1} |\langle \mathbf{f} \circ (T_i^\alpha \mathbf{g}_l)^*, \gamma_k \rangle|^2 \\
 &= N^\alpha \sum_{l=1}^L \sum_{i=1}^N \sum_{n=1}^N |\mathbf{f}(n)|^2 |(T_n^\alpha \mathbf{g}_l)(i)|^2 \\
 &= N^\alpha \sum_{n=1}^N |\mathbf{f}(n)|^2 \sum_{l=1}^L \|T_n^\alpha \mathbf{g}_l\|_2^2,
 \end{aligned}$$

where (15) follows from Parseval relation, the symmetry of \mathcal{L}_α and the definition of operator T_i^α . In addition, if $\sum_{l=1}^L |\hat{\mathbf{g}}_{l\alpha}(0)|^2 \neq 0$, we have

$$\begin{aligned}
 \sum_{l=1}^L \|T_n^\alpha \mathbf{g}_l\|_2^2 &= N^\alpha \sum_{p=0}^{N-1} \sum_{l=1}^L |\hat{\mathbf{g}}_{l\alpha}(r_p)|^2 |\gamma_p(n)|^2 \\
 &\geq \sum_{l=1}^L |\hat{\mathbf{g}}_{l\alpha}(0)|^2 > 0,
 \end{aligned}$$

taking the minimum and maximum of $\sum_{l=1}^L \|T_n^\alpha \mathbf{g}_l\|_2^2$, then we have the lower frame bound $A > 0$. Thus, \mathcal{G}_L^w is a frame with lower and upper frame bounds defined in (4) and (5).

APPENDIX B
PROOF OF COROLLARY 1

(15) From (6), the frame operator of $\mathcal{G}_{l\alpha}^w$ can be written as the diagonal matrix $S = \mathbf{D}_c = \text{diag}(\mathbf{c})$, with $c_n =$

$N^\alpha \sum_{l=1}^L \|T_n^\alpha \mathbf{g}_l\|_2^2 = C$ for $n = 1, 2, \dots, N$. Note that the optimal lower and upper frame bounds of a frame are the smallest and largest eigenvalues of the frame operator, respectively [24], the frame bounds of $\mathcal{G}_{l\alpha}^w$ are given by the smallest and largest entries in \mathbf{c} . Therefore, $\mathcal{G}_{l\alpha}^w$ is a tight frame if and only if \mathbf{c} is a constant vector; that is, there exists a constant C such that $c_n = C$ for $n = 1, 2, \dots, N$.

APPENDIX C
PROOF OF COROLLARY 2

In Appendix A, for any $\mathbf{f} \in \mathbb{C}^N$,

$$\begin{aligned} \sum_{l=1}^L \sum_{i=1}^N \sum_{k=0}^{N-1} |\langle \mathbf{f}, \mathbf{g}_{i,k}^{(l\alpha)} \rangle|^2 &= N^\alpha \sum_{n=1}^N |\mathbf{f}(n)|^2 \sum_{l=1}^L \|T_n^\alpha \mathbf{g}_l\|_2^2 \\ &= N^{2\alpha} \sum_{n=1}^N |\mathbf{f}(n)|^2 \sum_{p=0}^{N-1} \sum_{l=1}^L |\hat{\mathbf{g}}_{l\alpha}(r_p)|^2 |\gamma_p(n)|^2. \end{aligned} \quad (16)$$

Since the eigen-matrix γ of \mathcal{L}_α is orthogonal, we have $\sum_{p=0}^{N-1} |\gamma_p(n)|^2 = 1$, for $n = 1, 2, \dots, N$. If $\sum_{l=1}^L |\hat{\mathbf{g}}_{l\alpha}(r_p)|^2 = C$ for $p = 0, 1, \dots, N-1$, from (16), we have

$$\sum_{l=1}^L \sum_{i=1}^N \sum_{k=0}^{N-1} |\langle \mathbf{f}, \mathbf{g}_{i,k}^{(l\alpha)} \rangle|^2 = N^{2\alpha} C \|\mathbf{f}\|_2^2.$$

Thus, $\mathcal{G}_{l\alpha}^w$ is a tight frame with frame bounds $A = B = N^{2\alpha} C$.

APPENDIX D
PROOF OF PROPOSITION 1

The proofs of FMWGRFT, MWGRFT, MWGFT[25], WGRFT[34] and WGFT[17] are analogous. For the sake of convenience, we will only provide the proof for FMWGRFT. Note that the FMWGRFT matrix

$$FWf = N^\alpha \sum_{l=1}^L \gamma * ((\Psi^{l\alpha})^* \circ ((F \circ \gamma^H) * \gamma))^T.$$

As we all know, when α tends to 0, the graph fractional Fourier basis matrix γ tends to the identity matrix, i.e., $\lim_{\alpha \rightarrow 0} \gamma = I$. Then we have

$$\lim_{\alpha \rightarrow 0} FWf = \lim_{\alpha \rightarrow 0} \begin{pmatrix} \sum_{l=1}^L \mathbf{f}(1) \hat{\mathbf{g}}_{l\alpha}(r_0) & & 0 \\ & \ddots & \\ 0 & & \sum_{l=1}^L \mathbf{f}(N) \hat{\mathbf{g}}_{l\alpha}(r_{N-1}) \end{pmatrix}$$

We know that as α tends to 0, the vertex-frequency representation of FMWGRFT is clustered on the main diagonal, i.e., all values outside the main diagonal equal to 0.

APPENDIX E
PROOF OF THEOREM 2

Suppose that $\sum_{l=1}^L \hat{\mathbf{g}}_{l\alpha}^*(r_p) \hat{\mathbf{g}}_{l\alpha}(r_p) = \mu$ for $p = 0, 1, \dots, N-1$. Then we have

$$\begin{aligned} &\sum_{l=1}^L \sum_{i=1}^N \sum_{k=0}^{N-1} \langle \mathbf{f}, \mathbf{g}_{i,k}^{(l\alpha)} \rangle \tilde{\mathbf{g}}_{i,k}^{(l\alpha)} \\ &= N^{2\alpha} \sum_{m=1}^N \mathbf{f}(m) \sum_{l=1}^L \sum_{p=0}^{N-1} \sum_{p'=0}^{N-1} \hat{\mathbf{g}}_{l\alpha}^*(r_p) \hat{\mathbf{g}}_{l\alpha}(r_{p'}) \gamma_p^*(m) \gamma_{p'}(n) \\ &\quad \sum_{i=1}^N \gamma_p(i) \gamma_{p'}^*(i) \sum_{k=0}^{N-1} \gamma_k^*(m) \gamma_k(n) \\ &= N^{2\alpha} \sum_{m=1}^N \mathbf{f}(m) \sum_{l=1}^L \sum_{p=0}^{N-1} \sum_{p'=0}^{N-1} \hat{\mathbf{g}}_{l\alpha}^*(r_p) \hat{\mathbf{g}}_{l\alpha}(r_{p'}) \gamma_p^*(m) \gamma_{p'}(n) \\ &\quad \delta_{pp'} \delta_{mn} \\ &= N^{2\alpha} \mu \mathbf{f}(n). \end{aligned}$$

Thus, $\tilde{\mathcal{G}}_{l\alpha}^w$ is a dual of $\mathcal{G}_{l\alpha}^w$ with $C = \frac{1}{N^{2\alpha} \mu}$ in (9).

APPENDIX F
PROOF OF COROLLARY 3

If $\sum_{l=1}^L \hat{\mathbf{g}}_{l\alpha}^*(r_p) \hat{\mathbf{g}}_{l\alpha}(r_p) = \mu$ for $p = 0, 1, \dots, N-1$, by the Cauchy-Schwartz inequality, we have

$$\mu^2 = \left| \sum_{l=1}^L \hat{\mathbf{g}}_{l\alpha}^*(r_p) \hat{\mathbf{g}}_{l\alpha}(r_p) \right|^2 \leq \sum_{l=1}^L |\hat{\mathbf{g}}_{l\alpha}^*(r_p)|^2 \sum_{l=1}^L |\hat{\mathbf{g}}_{l\alpha}(r_p)|^2.$$

Then $\sum_{l=1}^L |\hat{\mathbf{g}}_{l\alpha}^*(r_p)|^2 \neq 0$ and $\sum_{l=1}^L |\hat{\mathbf{g}}_{l\alpha}(r_p)|^2 \neq 0$ for $p = 0, 1, \dots, N-1$. By Theorem 1, we have $\tilde{\mathcal{G}}_{l\alpha}^w$ is also a multi-windowed graph fractional Fourier frame.

APPENDIX G
PROOF OF COROLLARY 4

Suppose that S is the frame operator of $\mathcal{G}_{l\alpha}^w$. In the proof of Corollary 1, we have that $S = \mathbf{D}_c = \text{diag}(\mathbf{c})$. According to the definitions of frame and operator, the canonical frame of $\tilde{\mathcal{G}}_{l\alpha}^w$ is then given by

$$S^{-1} \mathbf{g}_{i,k}^{(l\alpha)} = \mathbf{D}_c^{-1} \mathbf{g}_{i,k}^{(l\alpha)} = \mathbf{D}_d \mathbf{g}_{i,k}^{(l\alpha)} = \mathbf{d} \circ \mathbf{g}_{i,k}^{(l\alpha)}.$$

APPENDIX H
PROOF OF THEOREM 3

We have

$$\mathbf{g}_{i,l} = \mathbf{D}_i S^\alpha \mathbf{g}_l,$$

where $\mathbf{D}_i = \text{diag}(\gamma_{1,i}, \gamma_{2,i}, \dots, \gamma_{N,i})$. Let $T_l = (\mathbf{D}_1 S^\alpha \mathbf{g}_l, \mathbf{D}_2 S^\alpha \mathbf{g}_l, \dots, \mathbf{D}_N S^\alpha \mathbf{g}_l)$, the corresponding synthesis operator of $\mathcal{G}_{l\alpha}^s$ can be expressed as $T = (T_1, T_2, \dots, T_L)$. We know that $\mathcal{G}_{l\alpha}^s$ forms a frame if and only if its frame operator is positive definite. In fact, the frame operator of $\mathcal{G}_{l\alpha}^s$ can be expressed as

$$S = \sum_{l=1}^L \sum_{i=1}^N [S^\alpha \mathbf{g}_l \mathbf{g}_l^* S^{\alpha*}] \circ (\gamma_i \gamma_i^*) = \sum_{l=1}^M [(S^\alpha \mathbf{g}_l) (S^\alpha \mathbf{g}_l)^*] \circ \mathbf{I}_N.$$

Here \mathbf{I}_N is an identity matrix. Let $\mathbf{G} = \sum_{i=1}^L \mathbf{g}_i \mathbf{g}_i^*$, we have

$$\sum_{l=1}^L (S^\alpha \mathbf{g}_l) (S^\alpha \mathbf{g}_l)^* = S^\alpha \mathbf{G} S^{\alpha*}.$$

Let \tilde{s}_k is the k th row of matrix S^α , the k th diagonal entry of $S^\alpha \mathbf{G} S^{\alpha*}$ can be written as $c_k := \tilde{s}_k \mathbf{G} \tilde{s}_k^*$. Therefore, $\mathcal{G}_{l\alpha}^s$ is a frame if and only if $c_k > 0$ for $k = 1, \dots, N$. The frame bounds of $\mathcal{G}_{l\alpha}^s$ are given by (12) which are the smallest and largest elements of \mathbf{c} .

APPENDIX I PROOF OF COROLLARY 6

By Theorem 3, the frame bounds of $\mathcal{G}_{l\alpha}^s$ are given by the smallest and largest elements in \mathbf{c} , with $c_k = \tilde{s}_k \mathbf{G} \tilde{s}_k^*$. Hence, $\mathcal{G}_{l\alpha}^s$ is a tight frame is then equivalent to the condition that $\tilde{s}_k \mathbf{G} \tilde{s}_k^* = C$ for $k = 1, \dots, N$.

REFERENCES

- [1] A. Sandryhaila and J. M. Moura, "Big data analysis with signal processing on graphs: Representation and processing of massive data sets with irregular structure," *IEEE Signal Process. Mag.*, vol. 31, no. 5, pp. 80–90, 2014.
- [2] L. Stanković and E. Sejdić, *Vertex-frequency Analysis of Graph Signals*. Springer, 2019.
- [3] A. Ortega, P. Frossard, J. Kovačević, J. M. Moura, and P. Vandergheynst, "Graph signal processing: Overview, challenges, and applications," *Proc. IEEE*, vol. 106, no. 5, pp. 808–828, 2018.
- [4] A. Sandryhaila and J. M. Moura, "Discrete signal processing on graphs: Frequency analysis," *IEEE Trans. Signal Process.*, vol. 62, no. 12, pp. 3042–3054, 2014.
- [5] E. Ceci and S. Barbarossa, "Graph signal processing in the presence of topology uncertainties," *IEEE Trans. Signal Process.*, vol. 68, pp. 1558–1573, 2020.
- [6] F. Gama, E. Isufi, G. Leus, and A. Ribeiro, "Graphs, convolutions, and neural networks: From graph filters to graph neural networks," *IEEE Signal Process. Mag.*, vol. 37, no. 6, pp. 128–138, 2020.
- [7] M. W. Morency and G. Leus, "Graphon filters: Graph signal processing in the limit," *IEEE Trans. Signal Process.*, vol. 69, pp. 1740–1754, 2021.
- [8] G. Leus, A. G. Marques, J. M. Moura, A. Ortega, and D. I. Shuman, "Graph signal processing: History, development, impact, and outlook," *IEEE Signal Process. Mag.*, vol. 40, no. 4, pp. 49–60, 2023.
- [9] J. Domingos and J. M. Moura, "Graph Fourier transform: A stable approximation," *IEEE Trans. Signal Process.*, vol. 68, pp. 4422–4437, 2020.
- [10] J. Jiang, C. Cheng, and Q. Sun, "Nonsampled graph filter banks: theory and distributed algorithms," *IEEE Trans. Signal Process.*, vol. 67, no. 15, pp. 3938–3953, 2019.
- [11] J. Jiang, D. B. Tay, Q. Sun, and S. Ouyang, "Design of nonsampled graph filter banks via lifting schemes," *IEEE Signal Process. Lett.*, vol. 27, pp. 441–445, 2020.
- [12] S. Chen, R. Varma, A. Sandryhaila, and J. Kovačević, "Discrete signal processing on graphs: Sampling theory," *IEEE Trans. Signal Process.*, vol. 63, no. 24, pp. 6510–6523, 2015.
- [13] S. Chen, A. Sandryhaila, J. M. Moura, and J. Kovačević, "Signal recovery on graphs: Variation minimization," *IEEE Trans. Signal Process.*, vol. 63, no. 17, pp. 4609–4624, 2015.
- [14] I. Jestrović, J. L. Coyle, and E. Sejdić, "A fast algorithm for vertex-frequency representations of signals on graphs," *Signal Process.*, vol. 131, pp. 483–491, 2017.
- [15] L. Le Magoarou and R. Gribonval, "Are there approximate fast Fourier transforms on graphs?" in *Proc. IEEE Int. Conf. Acoust., Speech Signal Process. (ICASSP)*. IEEE, 2016, pp. 4811–4815.
- [16] L. Le Magoarou, R. Gribonval, and N. Tremblay, "Approximate fast graph Fourier transforms via multilayer sparse approximations," *IEEE Trans. Signal Inf. Process. Netw.*, vol. 4, no. 2, pp. 407–420, 2017.
- [17] D. I. Shuman, B. Ricaud, and P. Vandergheynst, "Vertex-frequency analysis on graphs," *Appl. Comput. Harmon. Anal.*, vol. 40, no. 2, pp. 260–291, 2016.
- [18] —, "A windowed graph Fourier transform," in *Proc. IEEE Statist. Signal Process. Workshop (SSP)*. IEEE, 2012, pp. 133–136.
- [19] N. Linh-Trung, N. V. Dung, K. Abed-Meraim *et al.*, "A new windowed graph Fourier transform," in *Proc. NAFOSTED Conference on Information and Computer Science (NICS)*. IEEE, 2017, pp. 150–155.
- [20] R. Shafipour, A. Khodabakhsh, and G. Mateos, "A windowed digraph Fourier transform," in *Proc. IEEE Int. Conf. Acoust., Speech Signal Process. (ICASSP)*. IEEE, 2019, pp. 7525–7529.
- [21] H. Rabiei, F. Richard, M. Roth, J.-L. Anton, O. Coulon, and J. Lefèvre, "The graph windowed Fourier transform: a tool to quantify the gyration of the cerebral cortex," in *Workshop on Spectral Analysis in Medical Imaging (SAMI)*, 2015.
- [22] Y. Liu, F. Zhang, H. Miao, and R. Tao, "The hopping discrete fractional Fourier transform," *Signal Process.*, vol. 178, p. 107763, 2021.
- [23] L. Stanković, D. Mandić, M. Daković, B. Scalzo, M. Brajović, E. Sejdić, and A. G. Constantinides, "Vertex-frequency graph signal processing: A comprehensive review," *Digit. Signal Process.*, vol. 107, p. 102802, 2020.
- [24] P. G. Casazza and G. Kutyniok, *Finite Frames: Theory and Applications*. Springer Science & Business Media, 2012.
- [25] X. Zheng, C. Zou, L. Dong, and J. Zhou, "Multi-windowed vertex-frequency analysis for signals on undirected graphs," *Comput. Commun.*, vol. 172, pp. 35–44, 2021.
- [26] J. J. Healy, M. A. Kutay, H. M. Ozaktas, and J. T. Sheridan, *Linear Canonical Transforms: Theory and Applications*. Springer, 2015, vol. 198.
- [27] R. Tao, Y.-L. Li, and Y. Wang, "Short-time fractional Fourier transform and its applications," *IEEE Trans. Signal Process.*, vol. 58, no. 5, pp. 2568–2580, 2009.
- [28] R. Tao, B.-Z. Li, and Y. Wang, "Spectral analysis and reconstruction for periodic nonuniformly sampled signals in fractional Fourier domain," *IEEE Trans. Signal Process.*, vol. 55, no. 7, pp. 3541–3547, 2007.
- [29] L. Stanković, T. Alieva, and M. J. Bastiaans, "Time–frequency signal analysis based on the windowed fractional Fourier transform," *Signal Process.*, vol. 83, no. 11, pp. 2459–2468, 2003.
- [30] Y.-Q. Wang, B.-Z. Li, and Q.-Y. Cheng, "The fractional Fourier transform on graphs," in *Proc. Asia-Pacific Signal and Information Processing Association Annual Summit and Conference (APSIPA ASC)*. IEEE, 2017, pp. 105–110.
- [31] Y. Wang and B. Li, "The fractional Fourier transform on graphs: Sampling and recovery," in *Proc. IEEE International Conference on Signal Processing (ICSP)*. IEEE, 2018, pp. 1103–1108.
- [32] J. Wu, F. Wu, Q. Yang, Y. Zhang, X. Liu, Y. Kong, L. Senhadji, and H. Shu, "Fractional spectral graph wavelets and their applications," *Math. Probl. Eng.*, vol. 2020, no. 1, p. 2568179, 2020.
- [33] T. Alikashişoğlu, B. Kartal, and A. Koç, "Graph fractional Fourier transform: A unified theory," *IEEE Trans. Signal Process.*, vol. 72, pp. 3834–3850, 2024.
- [34] F.-J. Yan and B.-Z. Li, "Windowed fractional Fourier transform on graphs: Properties and fast algorithm," *Digit. Signal Process.*, vol. 118, p. 103210, 2021.
- [35] D. I. Shuman, S. K. Narang, P. Frossard, A. Ortega, and P. Vandergheynst, "The emerging field of signal processing on graphs: Extending high-dimensional data analysis to networks and other irregular domains," *IEEE Signal Process. Mag.*, vol. 30, no. 3, pp. 83–98, 2013.
- [36] R. A. Brown, M. L. Lauzon, and R. Frayne, "A general description of linear time-frequency transforms and formulation of a fast, invertible transform that samples the continuous s-transform spectrum nonredundantly," *IEEE Trans. Signal Process.*, vol. 58, no. 1, pp. 281–290, 2009.
- [37] Z. Yan and Y. Deng, "Single node reconstruction of graph signal based on graph fractional Fourier transform," in *Proc. International Conference on Signal Image Processing and Communication (ICSIPC)*, vol. 12246. SPIE, 2022, pp. 133–138.
- [38] F.-J. Yan and B.-Z. Li, "A new reconstruction formula and shift frame for WGFRT," in *Proc. International Conference on Signal Image Processing and Communication (ICSIPC)*, vol. 12916. SPIE, 2023, pp. 267–273.
- [39] G. B. Ribeiro, J. R. D. O. Neto, and J. B. Lima, "On the fractionalization of the shift operator on graphs," *IEEE Access*, vol. 10, pp. 16468–16478, 2022.